World Conference on
Timber Engineering
Oslo 2023

BURNING TEST OF STEEL BAR - TIMBER COMPOSITE BEAM

Shizuka Matsushita[1], Shinichi Shioya[2]

ABSTRACT: From a viewpoint of the current climate crisis, there has been much recent interest in using timber structural members in large buildings because timber can be used as renewable natural resource, and moreover, in severe earthquake prone zones, such as Japan, they are more desired on the grounds of light weight of timber members. We are developing a frame system consisting of hybrid timber members reinforced with deformed steel bar using epoxy resin adhesive. In order to practice the system, it is necessary to investigate fire resistance performance of the members. This paper reports a burning test of a beam burned for 60-minute semi-fireproof using burning marginal layer ,i.e., charring layer.

KEYWORDS: Fire, Burning marginal layer, Hybrid timber, Deformed steel bar, Beam

1 INTRODUCTION [3 4 5]

When constructing a large rigid-frame building with timber construction, the low bending stiffness and the low bending strength of timber become a serious problem.
S.Shioya, (author[2]) proposed a structural system for building construction, adopting Hybrid Glulam Timber members using Steel bar (HGTSB, nicknamed as "Samurai" in Japan) and has developed the structural design methodology, and constructed the first prototype building, a two-way frame structure using the structural system as seen in Figure 1 [1]. Three buildings were built with the system. One of them adapted two HGTSB beams, for a trial, at the 11th floor of a high-rise building, with a refractory coating authorized as two-hour fireproof timber for HGTSB, constructed in Tokyo, Japan, in February 2020. On the other hand, fireproof design method for using burning marginal layer (i.e. charring layer) for HGTSB is strongly desired for low-rise and middle-rise buildings. We scheduled to establish the semi-fireproof design method for HGTSB and conducted a fire resistance test of a beam.
The purpose of this study is to propose a method for estimating capacity of HGTSB beam that follows the semi-fireproof design method. A 60-minute burning test of a real-size beam was conducted. The safety factor, ratio of residual capacity of the beam after 60-minute burning divided by the loading expected under long-term loading, has not been sufficiently clarified. The safety factor is very important in the development of a new timber composite beam such as HGTSB. In the case of HGTSB, its bending strength is 3.0 to 4.0 times greater than that of timber beams, which means that the larger the cross-section, the greater the load on the beam, making it impossible to load the beam with Japanese burning test equipment. In such cases, if a method is established to estimate the safety factor of bearing resistance of the beam on the safe side, the burning test of the beam with its maximum cross-section is possibly eliminated.
Several studies [2,3] on fireproofing of carbon fibre-timber composite beam in which wood is used as main material, were conducted but there are no studies on fireproofing of steel bar-timber composite beam that use steel bar (i.e., rebar) as reinforcement against bending.
This paper reports the calculation concept for capacity of the beam during its burning, and the test to testify the concept and its results. Also, in another paper in WCTE2023, a new concept of modelling of temperature within beam with temperature data of only several measurement points is proposed [4].

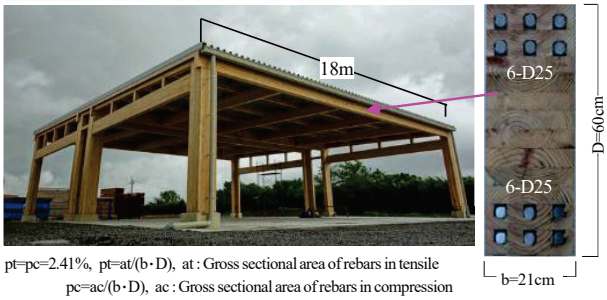

Figure 1: *Prototype building utilizing the hybrid beam and column proposed in this study, designed by S. Shioya with approval from authorities and constructed in July 2014*

[1] Shizuka Matsushita, Department of Architecture, Kagoshima University, Japan, k7422990@kadai.jp
[2] Shinichi Shioya, Department of Architecture, Kagoshima University, Japan, k7347039@kadai.jp

https://doi.org/10.52202/069179-0216

2 CALCULATION CONCEPT FOR BEAM CAPACITY

Resisting portion expected within a beam cross-section after 60-minute burning is illustrated in Figure 2(a).

1) Additional wood laminas of 90mm thickness are to be bonded to lower surface of the beam as fireproof for lower rebar within HGTSB beam.

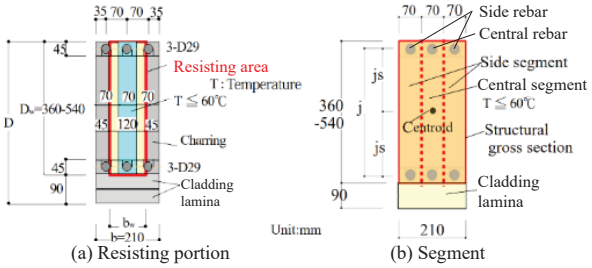

(a) Resisting portion (b) Segment

Figure 2: *An expected cross-section after 60 - minute burning and segments defined*

Table 1: *Rebar tensile properties*

Rebar	Er	σ_y	σ_t
D29	1.99×10^5	413	609

E_r:Young's modulus,
σ_y:Yielding modulus,
σ_{ty}:Tensile brealing strength (N/mm^2)

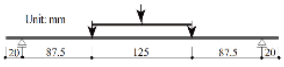

Figure 3: *Force for bending test*

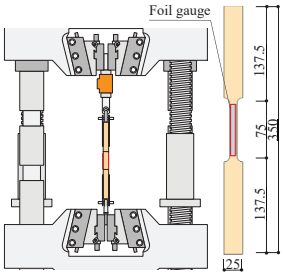

Figure 4: *Tensile test*

Table 2: *Mechanical properties of laminas*

No.	The number of pieces	Grade of Lamina	Bending test			Compression test		Moisture content	Block shearing test		
			Pure lamina		with joint	Pure lamina			n	Pure lamina	
			Ewb	σm	σm	Ewc	σm	%		τm	SD
L10	3	L80	8300	62.7	37.5	4026	30.3	12.3	-	N/A	
L9	3	L70	9000	66.9	N/A	6574	30.9	11.9	10	9.54	0.45
L8	3	L60	10700	61.7	45.0	3048	28.9	13.3	10	11.35	1.31
L7	3	L60	9400	62.7	N/A	5285	31.4	12.3	10	8.76	0.88
L6	3	L60	9100	57.2	N/A	5211	32.2	12.6	10	7.79	1.41
L5	3	L60	9700	54.8	N/A	3696	26.5	12.5	10	10.52	0.62
L4	3	L70	9400	65.6	51.0	4676	34.6	12.0	10	8.49	0.92
L3	3	L80	7400	46.5	49.7	3612	32.4	11.4	-	N/A	
L2	3	L60	7400	59.8	N/A	2682	29.7	11.9	10	12.50	2.86
L1	3	L60	9300	73.2	N/A	2715	35.4	12.3	10	11.78	2.19
Total	30	Average	8970	61.1	45.8	4152	31.2	12.2	80	10.22	1.33

E_{wb},E_{wc}: Young's modulus σ_w,τ_m: Strength SD:Standard deviation
n: The number of pieces

Table 3: *Assumed values and results for calculation of deflection under the initial cross-section before burning test*

D	b	Ewba	Er	Er/Ewba	Io	Ic	Ic/Io	κd	Gw
in mm		*in N/mm²*			*x10⁹*	*in mm⁴*			*in N/mm²*
450	210	8970	2.05×10^5	22.9	1.59	3.71	2.32	1.23	824
360					0.82	2.87	3.51	1.08	

E_{wba}: Average of E_{wb} in Table 2 $I_0 = b \cdot D^3/12$
κ_d: Shape factor for share deformation G_w: Modulus of shear elasticity

2) The resistance of the bonded laminas is not expected in the structural design.
3) Depth of charring layer is assumed to be 45mm after 60-minute burning.
4) Portion of area ($b_w \cdot D_w$) enveloped by red line is assumed to resist as wood.
5) The residual wood portion is assumed to resist at the allowable stress level for short-term loading.
6) Central segment of three segments equally divided in beam width as Figure 2(b) is assumed to resist as HGTSB because of its being cooler than allowable limit temperature (60°C) for HGTSB.

3 EXPERIMENT

3.1 SPECIMEN

Figure 6 in the next page illustrates cross-sections of specimen. Main cross section of the beam is Section II-IV with one-tier rebar lamina, which 3-rebars were embedded on the upper and the lower lamina of beam cross-section. Figure 5 illustrates a side view of the specimen and positions of strain gauge and thermocouple. The left-hand Section I is prepared to investigate effects of the amount and the numbers of rebars on elevated temperature of wood during burning.

The rebar laminas were prepared in the same way as in our previous paper [5]. The lamina was Cryptomeria Japonica; lamina composition of beam was adhered to Japanese Agricultural Standard E65-F225. Rebar diameter is D29(29mm) and its grade is SD390(Nominal yielding strength: $390N/mm^2$). Adhesive was typical resorcinol resin adhesive for laminating the laminas and epoxy resin adhesive for rebar, of which allowable upper limit temperature is 110°C.

3.2 YOUNG'S MODULUS, STRENGTH, AND MOISTURE CONTENT OF LAMINA

Table 2 lists mechanical properties of laminas by bending test, compression test, tensile test and block shear tests. Figure 3 shows applied force of the bending test. Compression tests were performed using specimens with cross section of 25 x 25 mm and height of 100 mm. Figure 4 shows configuration of the tensile test. The center length of 75mm was shaved down to 10 mm in width. Table 2 lists moisture content of lamina testpiece (45 x 210 x 20 mm), of which the numbers was three for each lamina. The shear plane for the block shear test were 26 x 36 mm. The numbers of specimens for these tests were 10 for each lamina.

Table 4: *Assumed values and results for calculation of bending moment capacity/Mu and shear capacity/Qws after burning, applied force/F and shear force/Q*

bw	Dw	Fw	fws	awt, awc	js	yt, yc	Iwo	Iw	Zw	Mwu	at, ac	fry	j	Mry	Mu	L/3	F/2	→	F	Q	fws	κs	Qws	Q/Qws
in mm		*in N/mm²*		*in mm²*		*in mm*	*x10⁸*	*in mm⁴*	*x10⁶*	*in mm³*	*in kN・m*	*in mm²*	*in N/mm²*	*in mm*	*in kN・m*		*in m*			*in kN*		*in kN*	*in N/mm²*		*in kN*	
120	360	22.5	15.0	1054	158	180	4.67	4.14	2.30		51.8	642.4	390	315	78.9	130.7	1.70	65.3	→	132	66.0	1.8	1.25	63.2	1.06

$M_u = M_{wu} + M_{ry}$ $M_{wu} = k_z \cdot Z_w \cdot f_{ws}$ $M_{ry} = a_t \cdot f_y \cdot j$ $Q_{ws} = f_{ws} \cdot b_w \cdot D_w \cdot / \kappa_s$ $Q = M_u/(L/3)$ j_s,j: See Figure 2 $y_t, y_c = D_w/2$ $I_{wo} = b_w^3/12$ $I_w = I_{wo} - (A_{wt} + A_{we}) \cdot (j/2)^2$

Table 5: *Results of calculation of stress of wood and rebar, and shear capacity under the initial cross-section before burning test*

D	b	M	Fw	rσy	kz	Mu	M/Mu	yt	yc	Zwt	Zwc	σ wbt	σ wbc	σ rt	σ rc	Q	κ s	τ m	fLa	τ m/fLa
in mm		*in kN・m*	*in N/mm²*			*in kN・m*		*in mm*		*x10⁶*	*in mm³*			*in N/mm²*		*in kN*			*in N/mm²*	
450	210	112.2	22.5	390	0.96	365	0.31	251	199	14.8	18.6	7.58	6.04	96	122	66.0	1.46	1.02	0.99	1.03
360					0.98	305	0.37	181	179	15.8	16.0	7.09	7.01	142	140		1.25	1.09		1.10

M= F/2・(L/3) = 66.7・1.7= 112.5kN・m $M_{wu} = k_z \cdot Z_w \cdot F_w$ $Z_{wt} = I_e/y_t$ $Z_{we} = I_e/y_c$ $\sigma_{wbt} = M/Z_{wt}$ $\sigma_{wbc} = M/Z_{wc}$ k_z: Size factor for bending strength of timber
y_t,y_c: Depth from centroid to upper fringe and lower fringe over beam σ_{rt},σ_{rc}: Stress of upper rebar and lower rebar

https://doi.org/10.52202/069179-0216

3.3 THE CENTER OF GRAVITY OF THE CROSS-SECTION AND SECTIONAL SECONDARY MOMENT OF BEAM

Using Young's modulus in bending for each lamina, distance/y_o from lower surface to the center of gravity of the cross-section and the cross-sectional secondary moment/I_e were calculated using Equation (1) and Equation (2) below.

$$y_o=(\Sigma n_{wi}\cdot a_{wi}\cdot y_{woi}+\Sigma(n_r-1)\cdot a_{ri}\cdot y_{roi}) /(\Sigma n_{wi}\cdot a_{wi}+\Sigma(n_r-1)\cdot a_{ri}) \quad (1)$$

$$I=\Sigma n_{wi}\cdot a_{wi}\cdot y_{woi}^2+\Sigma n_i\cdot I_{wi}+\Sigma(n_r-1)\cdot a_{ri}\cdot y_{roi}^2+\Sigma(n_r-1)\cdot I_{ri} \quad (2)$$

where, $n_{wi}=E_{wi}/E_{wo}$, $n_r=E_r/E_{wo}$, E_{wi} : Young's modulus in bending for each lamina, E_{wo}: Average value of all laminas, E_r: Young's modulus for rebar, a_{wi}, y_{woi} : Cross-sectional area of each lamina and distance from lower surface to the center of cross-section area of each lamina to origin, a_{ri}, y_{roi}: Cross-section area of each rebar and distance from lower surface to the center of cross-section of each rebar, I_{wi}: cross-sectional secondary moment of each lamina only ($=b\cdot t^3/12$), b: Lamina width, t: Lamina thickness, I_{ri}: Cross-sectional secondary moment of rebar ($Pi\text{-}d^4/64$), d: Diameter of rebar

Table 3 lists calculated values of the cross-sectional secondary moment/I_e, with and without considering fireproof laminas. I_e was 2.32 times greater than I_0 in the former case and 3.51 times greater in the latter case. Young's modulus/E_r and cross-sectional area/a_{r0} of the rebar were set to standard value ($E_r=2.05\text{x}10^5$ N/mm^2).

3.4 STRAIN AND TEMPERATURE MEASUREMENT

Figure 5(b) illustrates a side view of the beam specimen and positions of foil strain gauges and thermocouples. Figure 5(a) illustrates locations and names of the measured cross sections. It shows the locations where strain of wood and strain of rebar were measured. Numbering of mark "No." is for thermocouple; "W" is for uniaxial strain of wood in direction of beam axis, "R" is strain for rebar in the same direction. Figure 7(a) illustrates the gluing of foil gauge for wood. Before gluing laminas as beam, grooves were processed into laminas and the foil gauges were attached with adhesive for long-term measurement. The surface of the gauges was then coated with wax and was overwrapped with vinyl tape. Foil gauges were 3-wire type with lead wire temperature compensation. Thermocouples were used to measure temperature. Lead wire of the foil gauge and the thermocouple was pulled out from left or right end of the beam.

3.5 LOADING

Loading employed the four-point bending in Figure 8; magnitude of bending moment at mid-span of the specimen was selected to be value of allowable moment under long-term loading design. Value of shearing force of both side shear spans was 10% higher than its allowable shear force for long-term loading design. Force/F, vertical displacement, temperature, and strains of wood and rebar were measured. Deflections were measured for mid-span, two loading points, and both support points.

4 RESULT

4.1 HISTORY OF FORCE, TEMPERATURE, AND FRACTURES

The burning test was conducted on September 28, 2021 at 13:00 (its room temperature: 25.6°C) in a combustion furnace (ISO843-1 compliant furnace) at the Japan

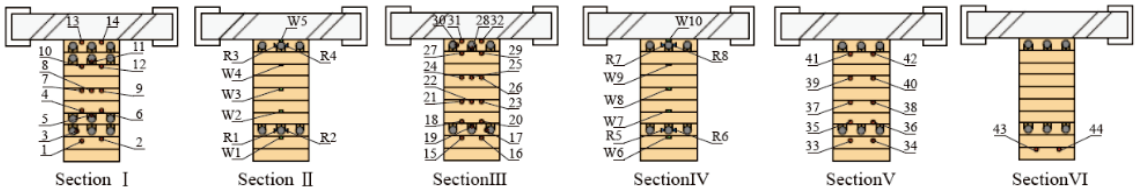

(a) *Locations of strain gauge and thermocouple*

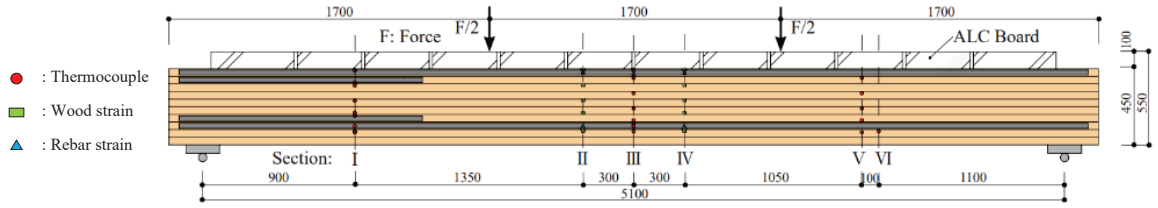

(b) *Side view of specimen*

Figure 5: *Side view of specimen and Locations of strain gauge and thermocouple*

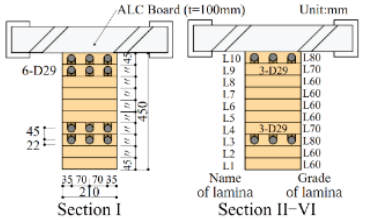

Figure 6: *Cross-sections of beam specimen*

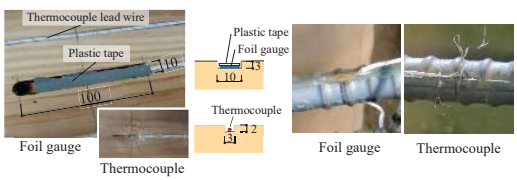

(a) *For wood* (b) *For rebar*

Figure 7: *Settlement of strain gauges and thermocouple*

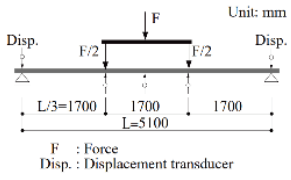

Figure 8: *The applied force and locations of deflection measurement*

https://doi.org/10.52202/069179-0216

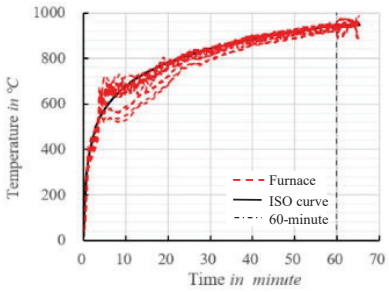

Figure 9: Temperature in furnace

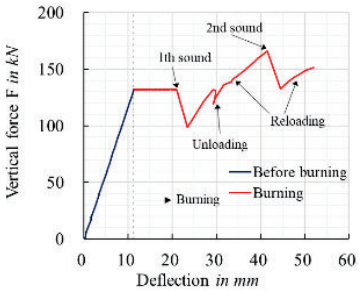

Figure 10: Force-deflection relationship

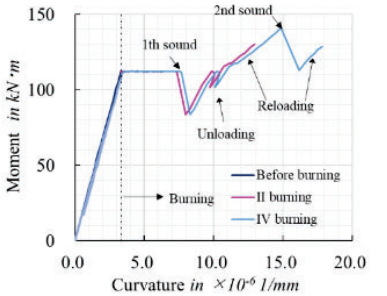

Figure 11: Bending moment-curvature relationship

Testing Center for Construction Materials. During introducing initial force, deflections and strains in the elastic range were measured. Figure 9 shows the heating temperature history of the air inside the furnace. After five minutes after completion of the loading, burning test was initiated. Temperature during 60-minute burning test was controlled to adhere to ISO-fire exposure temperature curve. Figure 12 shows changing of deflection at mid-span until the end of additional loading to investigate capacity after the burning. As burning proceeding, the deflection increases gradually, but an impact sound occurred suddenly just before 60-minutes passed, degrading the deflection stiffness, and ALC board over top of the specimen was found to be leaning.

At this time, it was confirmed that the capacity calculated by the concept mentioned in Chapter 2 was supported and the deflection of the mid-span was less than several thresholds for deflection required as semi-fireproof construction of the beam in Japan.

By reloading to the specimen at time of the impact sound before 60-minutes passed, the force F could again recover the initial applied force value, and then the additional loading was continued to be conducted. When the second impact sound occurred, the test was terminated because of the ALC board leaning largely. This additional time after the 60-minute burning passed was 5 minutes and 20 seconds; Temperature of the furnace was maintained at a constant temperature (945°C) by burning.

4.2 DEFLECTION - LOAD RELATIONSHIP DURING THE BURNING TEST

Figure 10 shows force-deflection relationship and Figure 11 shows bending moment–curvature relationship until the end of the burning test. The curvature is the same as that of the cross-section II and IV of Figure 15 mentioned later. Immediately after the first impact sound, the force decreased by 33.5kN; the deflection and curvature increased. The force increased to 166.2kN after 60-minute burning and decreased by 29.6kN at the second impact sound. The maximum force was 166.2kN, which was 26% higher than the initial force(F=132kN). The similar magnitude of the load drop immediately after the impact sounds is part of the evidence supporting the buckling of the upper two side rebar, which will be discussed in Section 4.6.

4.3 PERFORMANCE IN ELASTIC RANGE DURING INTRODUCTING INITIAL LOAD

Figure 13 shows strain distribution of wood and rebar of cross sections of II and IV during introduction the initial

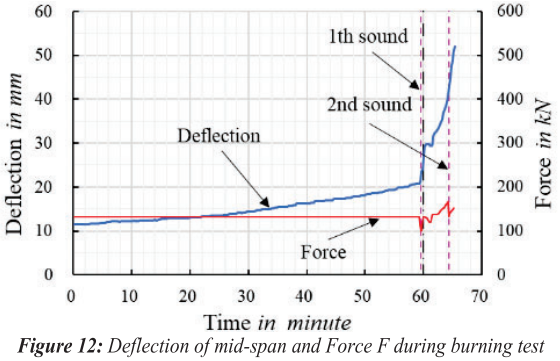

Figure 12: Deflection of mid-span and Force F during burning test

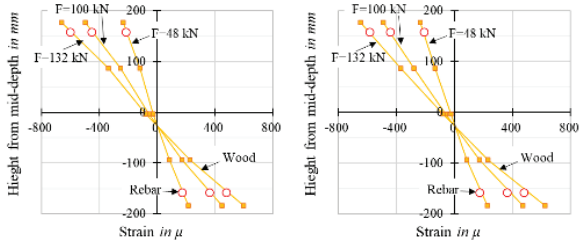

(a) Section II (b) Section IV

Figure 13: Bending strain profiles while introducing load

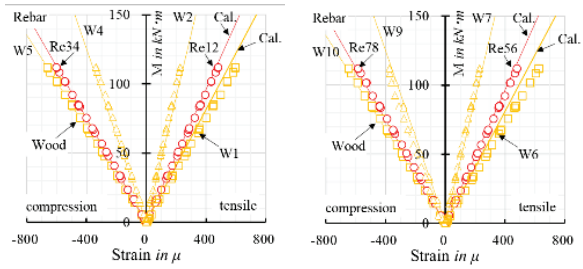

(a) Section II (b) Section IV

Experiment : □ , △ : Stain of wood ○ : Strain of rebar
Calculation: —— : Stain of wood —— : Strain of rebar

Figure 14: Comprision of calculation to experiment of bending moment-strain curves of timber surface and rebar

load. Strains of rebar are seen to be located on the line connecting the strain of wood, proving that rebar and wood in the same position within beam distort with same strain value. Figure 14 shows changing in the strain of the wood and rebar near lower or upper surface of beam, which are compared to those calculated using the plane section assumption in response to bending moment. The calculated values have approximately estimated the experimental values. Therefore, the assumption of the

https://doi.org/10.52202/069179-0216

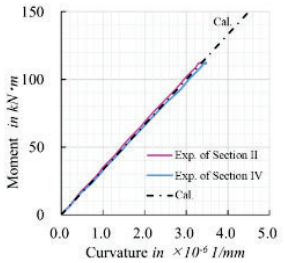

Figure 15: *Bending moment – curvature relationship*

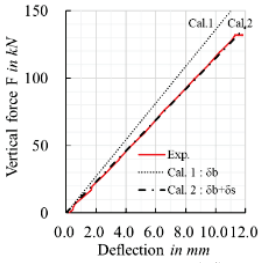

Figure 16: *Force-deflection relationship*

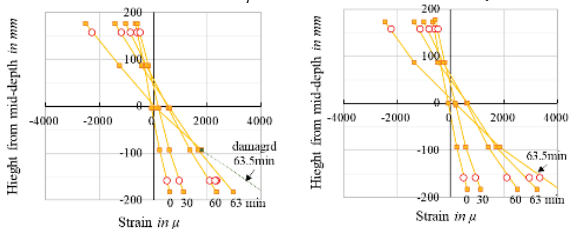

(a) Section II (b) Section IV

Figure 17: *Bending strain profiles during burning*

plane section is, also for RGTSB beam, confirmed to be allowed.

Figure 15 shows bending moment-curvature relationship for the cross-section II and IV. The curvature was assumed to be equal to average slope of strain distribution of wood cross section. The calculated bending stiffness is represented by a black one-dot chain line. The stiffness was calculated by I_e and E_{wba} in Table 3. Young's modulus of rebar was assumed to be its standard value. The bending moment-curvature relationships are almost same to the calculation line.

Figure 16 shows force-deflection relationship (red line) at the mid-span and relationships calculated using elastic stiffness. In the calculations, the fire cladding lamina was taken into account. Cal. 1 is deflection taking only bending deformation component/δ_b into account; Cal. 2 includes shear deformation component/δ_s. The coefficient of shear deformation /κ_d was assumed to be the value of 1.23 calculated by Eq. (10) in Reference [6]. The shear modulus of elasticity was not measured in this experiment, so the average value (824 N/mm^2) of the average value (15 pieces) of the center height of the beam web in Figure 24 of Reference [5]. In Figure 16, Cal. 2, which considers bending and shear deformation components, estimates the experimental relationship with high accuracy.

4.4 STRAIN DISTRIBUTION OF WOOD AND REBAR WITHIN BEAM DURING BURNING

Figure 17 shows strain distribution of wood and rebar at the cross section II and IV during burning. Amounts of strain increased with combustion proceeding resulted from decrease in resistance area within the beam as the combustion proceeding. In the Section II, at 63.5 min, strain value of rebar near the lower at 63.5min is small against wood strain distribution, i.e., black dotted line which was estimated on the basis of the trend of change up to that point because the wooden gauge at the lower could no longer be used for measurement. At the point of yielding in rebar, mill scale of rebar surface locally peels off and the adhesive around the rebar delaminates, resulting in stress relaxation in the rebar. This leads to variation in the strain of the rebar after the start of yielding. Excluding the variation of the effect, even after 60-minute burning, these results suggest that the assumption of plane in the cross section within the beam is reasonable.

4.5 DAMAGES AND CHARRING CONFIGURATION AFTER BURNING TEST

Photo 1(b) shows the specimen immediately after the burning test. The side rebars were supposed to be curved because of their buckling caused by thermal expansion in its axial direction during burning. When water was then poured on the specimen, temperature of the rebars decreased to room temperature and the rebars approached a straight line due to decay of thermal expansion, as shown in Photo 1(c). The specimen was applied to reveal capacity of the burnt specimen as mentioned later in Chapter 4. Figure 18(b), (c) shows cross-sections of residual wood portion over which its charring layer was removed after the additional loading test. Figure 18(d) shows lines of charring border of experiment and according to Eurocode 5 with a charring rate of 0.65 mm/min: red line is one of experimental results; blue line is line calculated assuming the combustion time reaching 60 minutes, and green line is line calculated assuming the combustion time reaching 65 minutes and 20 seconds.

(a) *Specimen before the burning test*

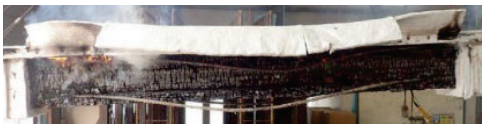

(b) *Specimen immediately after burning test*

(c) *Specimen cooled with water*

Photo 1: *Specimen*

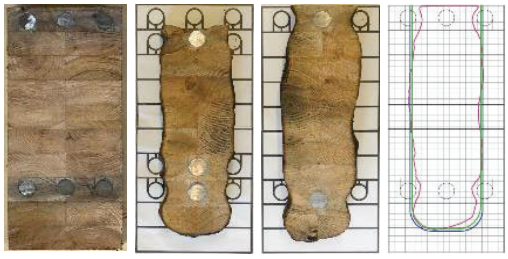

(a) (b) (c) (d)

(a)Cross-section of unburned portion
(b)Cross-section of Section I
(c)Cross-section of Section II-VI
(d)Curve of charring border
Red curve: experiment of (c),
Blue curve: Calculation by Eurocode with 60-min burning,
Green curve: Calculation by Eurocode with 65.3-min burning

Figure 18: *Cross-section of specimen after 65.3-minute burning*

https://doi.org/10.52202/069179-0216

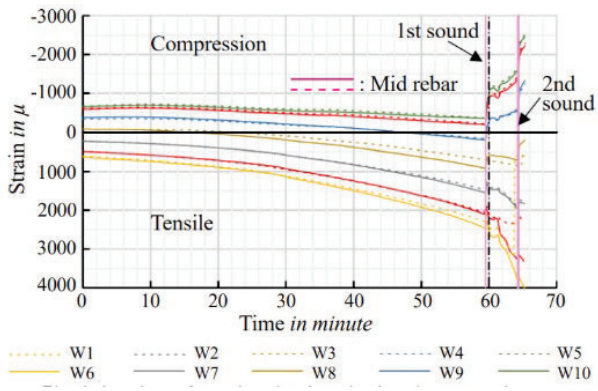

Figure 19: *Strains of wood and rebar Section II and IV*

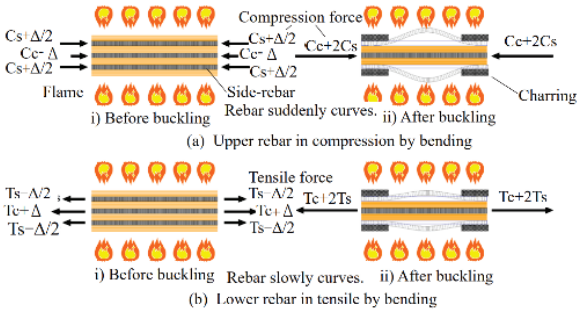

Figure 20: *Behavior of side-rebar curved during burning test*

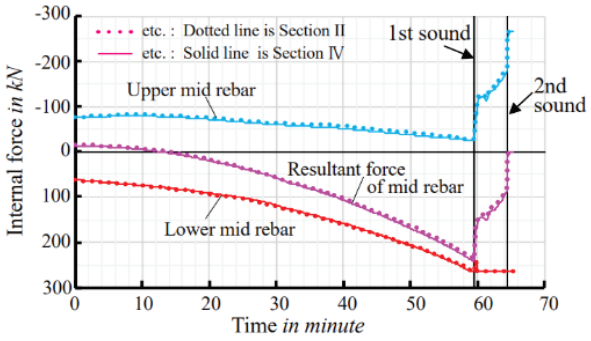

Figure 21: *Internal forces of mid rebar in Section II and IV*

Charring depth around the side rebar is larger than that of portion apart from the rebar. The reason may be that the side rebars buckled and some space generated between the rebar and wood by its curving. The side rebar is found to accelerate charring of wood in the case of 60-minute burning. The wood portion around the side rebar is necessary to be assumed not to contribute the capacity of beam at 60-minite burning on the safe side.

4.6 INFERENCE OF MECHANISM FOR THE IMPACT SOUND

Figure 19 shows changing in strains of wood and central rebar in the Section II and IV during burning: the dotted line indicates that of the Section II; the solid line indicates that of the Section IV; red line indicates that of the rebar. At the first impact sound, strain of the lower central rebar suddenly exceeded yielding strain (2075μ) of rebar, while the upper mid rebar reversed its trend of decreasing in compression and suddenly increased, exceeding the yielding strain (-2075μ) at the second impact sound. These suggest buckling of the upper side rebar, which is accompanied by impact sound.

Figure 20(a) shows schematically change in resistance of the upper rebars during burning. The upper rebar resists a greater compressive force due to bending moment of beam than that of the lower side rebar because it tries to extend axially during burning, whereas compressive force of the upper central rebar, which is lower in temperature than the side rebar, decreases. At the stage before the first impact sound, as seen in Figure 19, the strain of the upper central rebar (red solid and dotted lines) decreases in compression. Immediately after the first impact sound, the upper central rebar suddenly increased in compression strain and the reversal of velocity of strain changing can be seen to have occurred. These phenomena can be reasonably explained by the buckling of the side rebar. The reversal of strain velocity implies that the acceleration is great, which can be interpreted as a greater movement resulting in the impact sound; the similar amount of load drop after the two impact sounds, as discussed in Section 4.2, suggests that the load drop due to buckling of those two bars was of the same magnitude.

On the other hand, as the lower side rebar was subjected to tensile strain by bending, tensile force of the side rebar was gradually transferred to the lower central rebar from the start of burning, and even if the lower side rebar buckled due to axial extension, the velocity of movement of buckling is supposed to have been slow to the extend such that its acceleration was slow and did not lead to the motion that produced the impact sound.

4.7 EXTINCTION OF TEMPERATURE STRESS IN REBAR

Figure 21 shows changing of axial force of the upper (light blue line) and lower (red line) central rebar and resultant force (pink line) by sum of the axial forces. Dotted line indicates that of the Section II and thin line indicates that of the Section IV. The axial force was calculated by multiplying value of axial strain of the central rebar by nominal Young's modulus and cross-section. The resultant force (pink line) increases in tension from the start of burning but decreases at the first impact sound and reaches zero immediately after the second impact sound.

The reason for its becoming zero is that the lower central rebar yields in tension and the upper central rebar yields in compression, cross-section area of the rebars is identical, and the forces cancel each other. Because the side rebars have already buckled and are not resisting, the resultant force by rebars on the cross section of the timber will be zero at the section that fractures in bending. In other words, the component of bending moment resisted by the timber can be estimated using the properties of only wood taking into account the temperature increase,

https://doi.org/10.52202/069179-0216

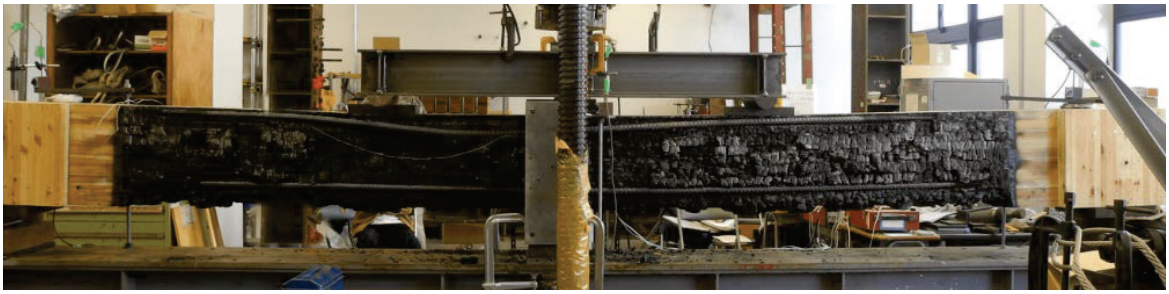

Photo 2: *Specimen before additional loading test burning test*

without the effect of the rebar. On the other hand, the component of bending moment resisted by the central rebar can also be estimated using on yield stress and sectional-area of rebar.

Bending capacity of the composite beam can be considered as the sum of these components. Rebar yields at approximately 0.2% of strain; then plastic flow occurs; the yield stress level is constant up to the start of strain hardening (about 2.0%). Assuming that the timber will fracture in bending, bending capacity of the beam can be estimated as the sum of both.

As can be seen in Figure 19, the rebars (red solid and dashed lines) almost strains in unison with wood portion (W1, W5, W6, and W10) around rebar until the rebar yielding. If yielding strain of rebar is smaller than rupture strain of wood at lower surface of beam and rebar is placed close to the surface, the assumption is satisfied. In this respect, HGSTB meets the requirements.

On the other hand, yield strain of rebar is about 0.2%, and fracture strain of wood in tensile by bending is expected to be approximately 0.4%, even if the wood ruptures at the finger joint of lamina.

However, the rupture strain is the value at room temperature. It may decrease at high temperatures. It is necessary to discuss the estimation of capacity at high temperature by considering the rupture strain of wood at high temperature.

4.8 LOADING TEST AFTER BURNING TEST

Because the additional loading immediately after the burning test did not reveal capacity of the specimen owing to the limitation of the loading apparatus, loading test was conducted to reveal the capacity as shown Photo 2 at Kagoshima University laboratory on February 15, 2022, i.e., 4.5 months after the burning test.

The force was the same as those of the burning test. Figure 22 shows the force-deflection relationship with a black curve. Figure 23 shows the bending moment-curvature relationship at the mid-span as yellow and black curves.

Those are overlaid on Figure10 and Figure 11. Yellow curve is with curvature by strain of wood; black curve is curvature by strain of rebar. In Figure 23, the stiffness of the curvature of rebar was reduced at the point indicated by '○'. In Figure 22, the point is also indicated with the same symbol, where the deflection stiffness also decreases.

Photo 3 shows failure of the upper of beam. When the capacity of beam decreased, wood portion at the force

Photo 3: *Partial compressive deformation around loading plat*

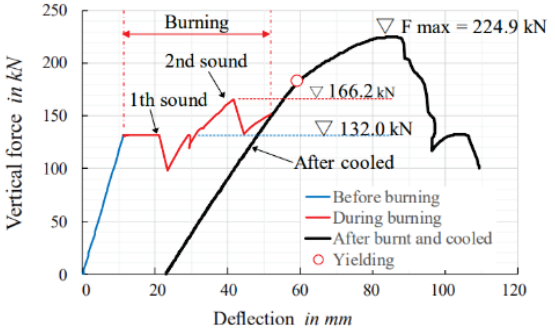

Figure 22: *Force-deflection relationship after cooled*

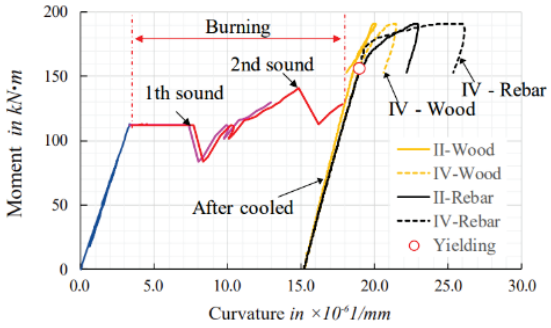

Figure 23: *Bending moment-curvature relationship after cooled*

position became more dented, causing the left side of the upper portion to bounce up.

In Figure 22, the maximum force of 166.2kN in the burning test is indicated with red dotted horizontal line. The force value was 73.9% of the maximum force in this test (F=224.9kN); this means that bending capacity of the specimen could not have been measured by during additional loading just after the 60-minute burning test.

The maximum capacity was 170.4% of the long-term loading load (132kN); this means that the capacity of specimen was sufficient against the collapse of the specimen in the 60-minute burning test.

https://doi.org/10.52202/069179-0216

These experimental results suggest that the approach for calculation of capacity proposed in Chapter 2 has sufficient potential to estimate bending and shear capacity of steel bar - timber composite beam just after 60-minute burning on the safe side.

5 SUMMARIES

In order to establish a design method for semi-fireproof for steel bar-timber composite beam, a 60-minute burning test was conducted, clarifying temperature [4] and strain behaviour inside the beams. The following i) to ii) were found during loading before the burning test, and iii) to vi) were found by the 60-minute combustion test and additional loading test to its specimen cooled after the burning test.

i) Detailed strain measurements of the wood and rebar within the specimen showed that rebar and wood in the same position within beam subjected bending distort with same strain value, providing a basis for the assumption of plane section within the composite beam's cross-section.

ii) Bending stiffness calculated based on assumption of the plane section within beam subjected to bending and using Young's modulus in bending of each lamina within beam specimen could estimate accurately moment-curvature relationship of the beam and changes in strain of wood and steel bars within the beam. Deflection stiffness of the composite beam was also accurately estimated by adding shear deformation to bending deformation component.

iii) Burning tests confirmed that a steel rebar-timber composite beam specimen bonded with two laminas (sum thickness of 90 mm) at the lower surface of beam exhibited bending and shear capacities calculated using the proposed resistance section model even after 60 minutes of burning.

iv) After 60 minutes of burning, load was increased with continuing the burning, and it was confirmed that the specimen could withstand up to 126% of the long-term allowable load. Furthermore, the specimen was cooled and subjected to loading test, and it was confirmed that load reached a maximum of 170.4% of the allowable long-term load and then collapsed. It was confirmed that the proposed estimation method for capacity of the beam after 60-minute burning is sufficient to estimate load capacity of timber-rebar composite beam on the safe side.

v) Although during 60-minute burning test, a component of elongation was added to upper central rebar and lower central rebar within beam width owing to the difference in temperature between surface portion and interior portion within beam, and with buckling of the upper side-rebar, the addition changed abruptly, causing the central rebars to yield before reaching the bending capacity and the thermal stress in the wood and rebar beam extinct.

vi) Charring depth for 60-minute burning wood was in approximately close agreement with the Eurocord 5 value. However, it should be taken into account that the depth is greater around the side rebar.

ACKNOWLEDGEMENT

This project was funded as Grants-in-Aid for Scientific Research-B by Japan Society for the Promotion of Science.

LITERATURES

[1] S. Shioya: Hybrid timber-steel bar glulam and its building system, JTCCM, JOURNAL Vol. 52, 2-7, 2016.8 (in Japanese)

[2] T G. Williamson, B Yeh: Fire performance of FRP reinforced glulam, MEETING THIRTY-NINE FLORENCE, ITALY, August, 2006

[3] Abdulrahman Zaben, et al. : Residual performance of a prototype hybrid timber-FRP glulam beam after fire, Santiago, Chile, WCTE 2021

[4] S. Matsushita, S. Shioya: A new method for modeling temperature within steel bar - timber composite beam using data by burning test, Oslo, WCTE 2023

[5] Kazuya Mori, Shinichi Shioya: Stiffness and strength of full-scale steel bar-timber composite beams with comparative small-depth, Santiago, WCTE 2021

[6] N. Fukutomi, S. Shioya: Design method to estimate stiffness and strength of hybrid timber-steel bar beams, Seoul, WCTE 2018

https://doi.org/10.52202/069179-0216